AIP | Journal of Applied Physics

Nitrogen plasma treatment of fluorine-doped tin oxide for enhancement of photo-carrier collection in amorphous Si solar cells

Seung Jae Baik and Koeng Su Lim

Citation: J. Appl. Phys. **109**, 084506 (2011); doi: 10.1063/1.3572262
View online: http://dx.doi.org/10.1063/1.3572262
View Table of Contents: http://jap.aip.org/resource/1/JAPIAU/v109/i8
Published by the American Institute of Physics.

Nitrogen plasma treatment of fluorine-doped tin oxide for enhancement of photo-carrier collection in amorphous Si solar cells

Seung Jae Baik[a] and Koeng Su Lim
Department of Electrical Engineering, Korea Advanced Institute of Science and Technology (KAIST), 291 Daehak-ro, Yuseong-gu, Daejeon 305-701, South Korea

(Received 22 September 2010; accepted 21 February 2011; published online 21 April 2011)

Nitrogen plasma treatment was performed on fluorine-doped tin oxide (SnO_2:F) front electrodes, and its impact on the performance of *pin* type amorphous Si (a-Si) solar cells was investigated. Nitrogen plasma treatment reverses the surface band bending of SnO_2:F from accumulation to depletion, thus in turn reversing the band bending of the p type amorphous silicon carbide (p-a-SiC) window layer. The reversal of band bending leads to the collection of carriers generated in p-a-SiC, and quantum efficiency in the short wavelength regime is thereby enhanced. On the other hand, surface depletion of SnO_2:F causes a reduction of the diode built-in voltage and increased series resistance, which could degrade the open circuit voltage (Voc) and fill factor (FF), the degradation of which is strongly affected by the deposition time of p-a-SiC. © *2011 American Institute of Physics*. [doi:10.1063/1.3572262]

I. INTRODUCTION

From a theoretical point of view, carrier collection in *pin* type a-Si solar cells with a sufficiently thick absorber layer mainly depends on the collection length of the intrinsic absorber layer and light absorption at the p type window layer. The collection length of the absorber layer depends on the mobility-lifetime product ($\mu\tau$) and the built-in voltage of the *pin* diode where the former can be enhanced by high quality a-Si thin films with low defect densities, and the latter depends on the work function of doping layers. Therefore increasing the doping density of the p-a-SiC window layer could enhance the carrier collection of solar cells; however, the light absorption increases with an increase of doping density of p-a-SiC.[1]

Light absorption in p-a-SiC cannot contribute to the output photocurrent because the direction of the internal electric field at p-a-SiC is opposite to the direction of carrier collection.[2] Accordingly, several efforts to reduce light absorption in the p type window layer have been reported. Higher bandgap materials such as amorphous silicon oxide,[3] amorphous carbon,[4] and amorphous silicon nitride[5] have been reported. Although these materials have a higher optical bandgap than p-a-SiC, their band alignment with intrinsic amorphous Si (i-a-Si) and/or work function is not appropriate for Voc and FF enhancement. Meanwhile, insertion of a wide-gap material between the front electrode and p-a-SiC was reported to enhance solar cell performances,[6,7] where the enhancement was attributed to reduced band bending of p-a-SiC.

Furthermore, it was recently pointed out that photo-generated carriers in p-a-SiC can be extracted by the reversal of band bending of p-a-SiC implemented by nitrogen plasma treatment of Al-doped ZnO.[8] In this work, we present the effect of nitrogen plasma treatment on SnO_2:F and show that similar carrier collection enhancement to that of Al-doped ZnO can be obtained. In addition, the origin of Voc and FF degradation, which is dependent on the deposition time of p-a-SiC, is discussed in detail.

II. EXPERIMENTAL METHODS

Nitrogen plasma treatment was performed on surface textured SnO_2:F glass (Asahi U-type) with a multichamber plasma enhanced chemical vapor deposition system for 10 min at 250 °C, 0.8 Torr, and under radio frequency power of 100 W with an electrode diameter of 8 in. Using the same plasma enhanced chemical vapor deposition system, p-a-SiC layers with various thickness splits were deposited on SnO_2:F glass, and a 250 nm layer of intrinsic a-Si (i-a-Si) and a 20 nm layer of n-type microcrystalline Si (n-μc-Si) were subsequently deposited. The detailed deposition conditions are listed in Table I. The dark conductivity of p-a-SiC was 3.4×10^{-6} S/cm. Finally, an array of rectangular Al back electrodes was evaporated with each having an area of 0.09 cm^2. Photocurrent density versus voltage measurement was taken under irradiation conditions of AM 1.5G and 75 mW/cm^2. A constant energy spectrophotometer was used for the quantum efficiency (QE) measurements with the incident photon power of 50 μW/cm^2, and an x-ray photoelectron spectroscopy (XPS) analysis was performed with an Mg Kα x-ray source. All electrical measurements were carried out at room temperature.

III. RESULTS AND DISCUSSION

A. Nitrogen plasma treated SnO_2:F

To reveal the chemical changes of SnO_2:F induced by the nitrogen plasma treatment, an XPS analysis was performed for untreated, nitrogen plasma treated (N-treatment), hydrogen plasma treated (H-treatment), and nitrogen-hydrogen serially treated (NH-treatment) SnO_2:F. N treatment was

[a]Author to whom correspondence should be addressed. Electronic mail: solar100@kaist.ac.kr.

TABLE I. N-treatment and deposition conditions (B_2H_6 and PH_3 are diluted in H_2).

	Gas flow rate (sccm)	Temperature (°C)	Pressure (torr)	Power (W)	Deposition time
N-treatment	$N_2 = 20$	250	0.8	100	10 min
p-a-SiC	$SiH_4/H_2/1\%\ B_2H_6/CH_4 = 1/9/0.5/0.6$	210	1	9	20, 40, 60, 80 s
i-a-Si	$SiH_4/H_2 = 10/11$	250	0.8	24	20 min
n-μc-Si	$SiH_4/H_2/1\%\ PH_3 = 1/200/2.1$	250	0.8	55	20 min

performed with 100 W power as noted in Sect. II, and H-treatment was performed at the same power, pressure, and temperature conditions as used for p-a-SiC deposition to simulate the surface chemical changes of SnO_2:F occurring during p-a-SiC deposition. Sn3d spectra shown in Fig. 1(a) reveal a typical 487 eV peak for the untreated sample; the peak shifts to a lower binding energy, and an additional tail near 485 eV appears with hydrogen plasma treatment due to the chemical reduction of SnO_2.[9] In addition, the N- and NH-treated samples exhibit similar peak positions with the reference sample and with greatly reduced intensities. This implies vaporization of Sn atoms possibly through the formation of volatile products containing carbon atoms. Markedly reduced intensity of C1s for the N- and NH-treated samples shown in Fig. 1(d) supports this argument. Moreover, the O1s spectra also show chemical shifts with N-treatment toward higher binding energy. Kunat *et al.* suggested that the O1s spectra of ZnO with higher binding energy correspond to O-H bonding.[10] In this regard, for the case of SnO_2:F, the appearance of a tail at higher binding energy with H treatment could be attributed to the formation of O-H bonds, and N- and NH- treatment may cause Sn-O bonds to change to O-H bonds in combination with Sn vaporization. In Fig. 1(c), the N1s peak at 398 eV can be attributed to nitrogen incorporation,[11,12] and these nitrogen atoms may substitute Sn atoms, which were vaporized by high power plasma treatment. To sum up, N- or NH- treatment causes surface Sn desorption and leaves nitrogen and oxygen in the form of adsorbed species on the surface of SnO_2:F. This might suppress the surface carrier concentration of SnO_2:F and, in turn, provide a surface depletion condition for SnO_2:F.

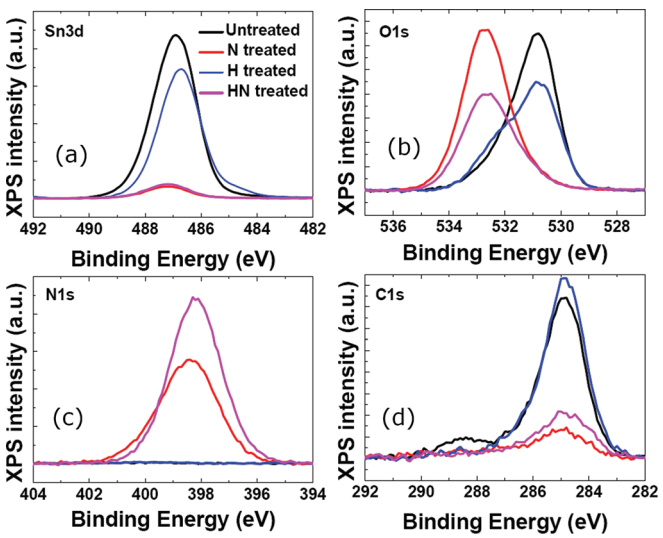

FIG. 1. (Color) XPS (a) Sn3d (b) O1s (c) N1s and (d) C1s spectra of untreated (black), N-treated (red), H-treated (blue), and NH-treated (magenta) SnO_2:F.

B. Enhancement of quantum efficiency

Figures 2(a) and 2(b) show the QE enhancement of solar cells with N-treatment. QE spectra for different p-a-SiC thicknesses decrease in magnitude as the p-a-SiC deposition time is increased from 20 to 80 s. To investigate the possibility of material change of p-a-SiC due to nitrogen back diffusion, we have evaluated the optical transmittance and XPS spectra for samples comprising 10 nm p-a-SiC (60 s deposition) on SnO_2:F with and without N treatment. We did not find a significant difference in optical transmittance and XPS spectra, thus implying that QE enhancement with N-treated SnO_2:F is not related to the reduced absorption of p-a-SiC or SnO_2:F. Moreover, the surface texture of SnO_2:F did not show any change from the scanning electron microscopy observations or the measurement of diffuse transmittance. Accordingly, the enhancement of QE can be attributed to enhanced carrier collection. This may be due to change of the band bending condition at the interface of SnO_2:F/p-a-SiC; more specifically, we could assume there is a band bending reversal of p-a-SiC.[8]

To estimate the percentage of carrier collection at the p-a-SiC layer, the QE spectra of a solar cell without p-a-SiC were measured as shown in Fig. 3. For the cell with p-a-SiC deposition time of 20 and 60 s, the quantum efficiency of carrier collection at the p-a-SiC layer was estimated to be around 80 and 20%, respectively. Utilizing the relation formulated by Crandall, that is, $QE = l_c/L[1 - \exp(L/l_c)]$, where l_c is the collection length and L is the absorber thickness,[13] the QE is determined to be 0.632 when the collection length is similar to the absorber length. Therefore as a rough estimate, the collection length of the p-a-SiC in our experiment is smaller than 10 nm, considering that the measured thickness of the p-a-SiC sample with 60 s deposition was 10 nm.

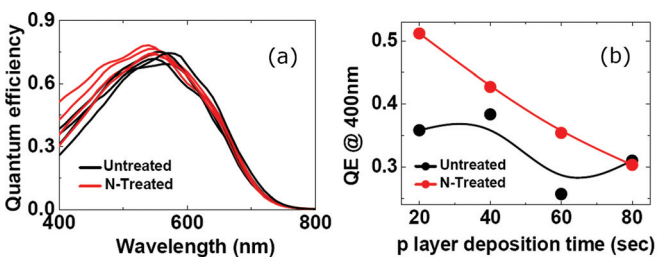

FIG. 2. (Color online) (a) QE spectra of cells with untreated and N-treated SnO_2:F. Four data lines for each color are obtained from four different thicknesses of p-a-SiC (deposition time of 20, 40, 60, and 80 s). (b) QEs at 400 nm are selected from each line of (a) and plotted with p-a-SiC deposition time.

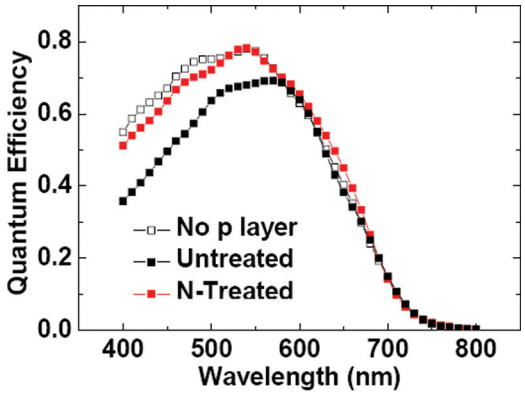

FIG. 3. (Color online) QE data comparison among cell with no p layer, a 20 s deposited p layer on untreated SnO_2:F, and a 20 s deposited p layer on N-treated SnO_2:F.

C. Fill factor and open circuit voltage

Figure 4 shows solar cell output parameters versus p layer deposition time for N-treated and untreated samples. Short circuit currents (Jsc's) are enhanced for N-treated samples and become similar when p layer deposition time increases up to 80 s, consistent with QE spectra shown in Figs. 2(a) and 2(b). The decrement of Jsc enhancement with an increase of p layer thickness can be explained by the limited collection length of p-a-SiC as noted in Sect. III.B. The FF of the N-treated samples drastically decreases with a decrease of p layer deposition time. This is attributed to an increase of the series resistance (R_s) as shown in Fig. 5, where R_s is extracted from the dark current versus voltage characteristics. The increase of R_s is due to reduced tunneling probability at the surface depleted SnO_2:F/p-a-SiC interface, which can be visually understood from Fig. 6. The tunneling current at the interface can be represented by the following equation[8]:

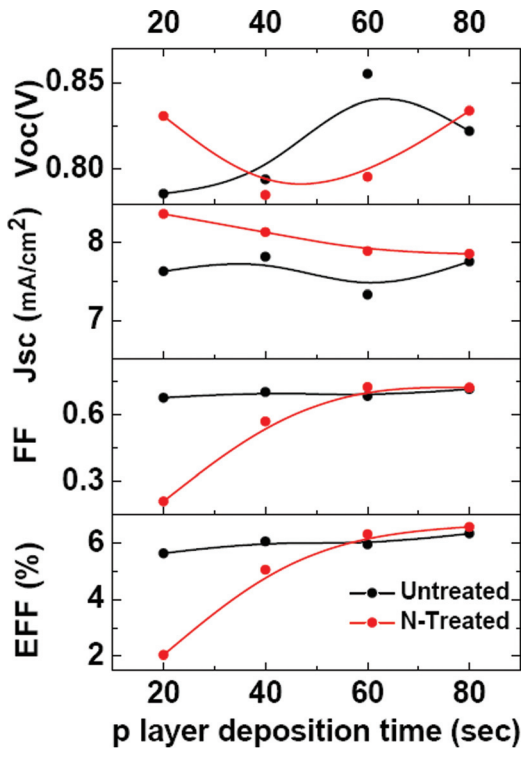

FIG. 4. (Color online) Solar cell output parameters vs p layer deposition time for cells with and without N-treatment.

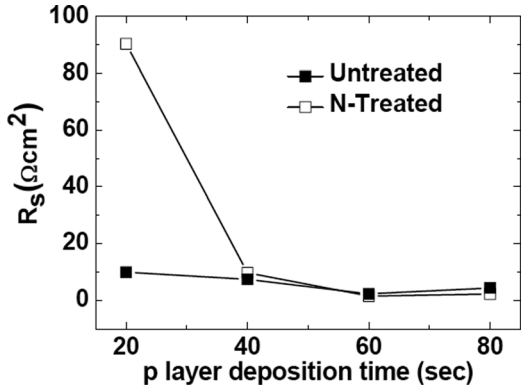

FIG. 5. Series resistance vs p layer deposition time for cells with and without nitrogen plasma treatment. Series resistance values were extracted from a dV/dJ vs 1/J plot; the detailed extraction procedure has been reported elsewhere.[14]

$$\frac{J_c}{q} \cong n_z N_t P^* [1 - f(E_t)], \tag{1}$$

where n_z is the free electron concentration at SnO_2:F, $f(E)$ is the Fermi–Dirac distribution function, E_t is the averaged energy level of traps in p-a-SiC, N_t is the trap density at p-a-SiC, and P^* is the tunneling probability. Considering that n_z, N_t, and $f(E_t)$ in Eq. (1) do not change on a large scale with band bending conditions, the decrease of surface depletion at SnO_2:F implies an increase of P^*. As the deposition time of p-a-SiC is increased, the surface of SnO_2:F is exposed to atomic hydrogen for longer time. Even though the surface of SnO_2:F is covered by a few nanometer p-a-SiC layer, hydrogen radicals can easily diffuse through and reduce the surface of SnO_2:F; thus the surface carrier concentration could increase again as the p-a-SiC deposition time is increased.[15–17] Therefore when the thickness of p-a-SiC is as high as that shown in Fig. 6(b), the surface depletion of SnO_2:F could be reduced.

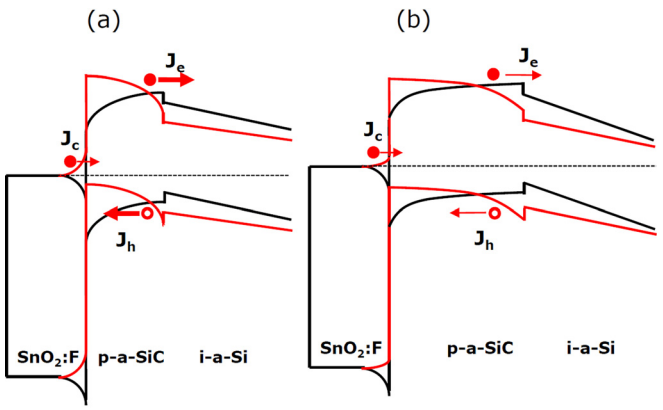

FIG. 6. (Color) Band diagram showing the model for thin p-a-SiC (corresponding to the deposition time of 20 s) (a), and for thick p-a-SiC (corresponding to the deposition time of 60 s (b). Black lines represent the case for no plasma treatment, and red lines represent the case for nitrogen plasma treatment. J_c is the tunneling current at the interface between SnO_2:F and p-a-SiC. J_e and J_h are the electron and hole current representing the charge separation in the p-a-SiC layer.

Accordingly, R_s would decrease, which could explain the dependence of R_s on p layer deposition time.

The trend of Voc according to p-a-SiC deposition time stems from a combination of three different mechanisms. First, highly resistive contact between SnO_2:F and thin p-a-SiC raise Voc with N treatment due to suppressed leakage for the case of p-a-SiC deposition time of 20 s. Second, V_{bi} degradation induced by reversed band bending of p-a-SiC lowers Voc for the case of p-a-SiC deposition time of 60 s.[8] Third, overexposure to hydrogen plasma would change the surface of SnO_2:F toward carrier accumulation, and consequently the band-reversal of p-a-SiC is restored for the case of p-a-SiC deposition time of 80 s. Overlapping of these three mechanisms can be represented by a U-shaped trend as shown in Fig. 4.

Figure 6 shows how the band bending of the SnO_2:F surface affects the band alignment of the p/i interface. When the SnO_2:F surface is carrier depleted, the band edges of p-a-SiC at the SnO_2:F surface are lifted to meet Anderson's rule, and thus the band bending of p-a-SiC is reversed compared to the case that the SnO_2:F surface is carrier accumulated. The curvature of band bending should be the same irrespective of the surface band bending condition of SnO_2:F because the space charge density is the same and the p-a-SiC layer can be assumed to be fully depleted in both cases. Accordingly, when the surface of SnO_2:F is depleted, the electron potential at the band edges of p/i interface becomes smaller than the case with surface accumulated SnO_2:F. This leads to the smaller built-in electric field on i layer as represented by reduced slopes of band edges as shown in Figs. 6(a) and 6(b). In addition, reversed band bending in p-a-SiC drives carrier separation of photo-generated carriers as indicated by J_e and J_h in Fig. 6. Moreover, the surface band bending of SnO_2:F when p-a-SiC is think as shown in Fig. 6(b) is smaller than when p-a-SiC is thin as shown in Fig. 6(a), which represents the reduction effect of SnO_2:F surface for thick p-a-SiC deposition. Therefore when the thickness of p-a-SiC is increased, the internal potential drop across the p-a-SiC is decreased, and thus the carrier separation in p-a-SiC becomes less pronounced.

In the case of a N-treated cell, injection of additional electrons from the p-a-SiC into the i-Si affects recombination statistics in i-Si. To further characterize regarding this, bias dependent QE measurement at a wavelength of 650 nm was performed as shown in Fig. 7(b). Figure 7(a) represents the coordinate and boundary conditions for the carrier concentration at p/i and n/i interfaces. A low light intensity of 50 μW/cm^2 was used in our QE measurement, and thus uniform electric field on i layer can be assumed.[13] In addition, constant generation rate throughout i-Si can be assumed because weakly absorbed light (wavelength: 650 nm) is used in the QE measurement.[13] Therefore diffusion current can be neglected and the current density J can be represented as follows:

$$\frac{J}{q} = pv_p + nv_n = p_0v_p + n_0v_n = n_Lv_n, \tag{2}$$

where p and n are hole and electron density varying with position; v_p and v_n are hole and electron drift velocity; p_0 and

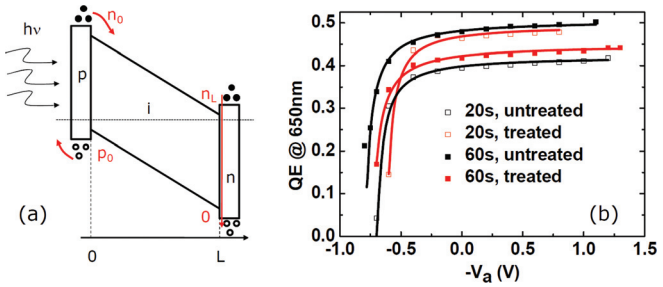

FIG. 7. (Color) (a) Simplified illustration of band diagram with boundary carrier concentrations are indicated. (b) QE at 650 nm vs applied voltage on SnO_2:F. Symbols denote experimental data, and lines denote fitted data.

n_0 are hole and electron density at p/i interface; n_L are electron density at n/i interface. Equation (2) has a similar form with Crandall's reports except the additional term n_0, which was regarded as zero by Crandall,[13] but n_0 should be added in this work to investigate the effect of carrier injection from the p layer into the i layer. Assuming constant lifetime regional approximation,[13] we can obtain the similar form of QE with effective collection length l_c^* as follows:

$$QE = \frac{l_c^*}{L}\left[1 - \exp\left(-\frac{L}{l_c^*}\right)\right]$$

$$l_c^* = l_p^* + l_n = \frac{l_p}{1 - \frac{n_0}{n_L}} + l_n = (\mu\tau)^*(-V_a + V_{bi})/L$$

$$(\mu\tau)^* = \frac{(\mu\tau)_h}{1 - \frac{n_0}{n_L}} + (\mu\tau)_e, \tag{3}$$

where L, l_p, and l_n are thickness of i layer, hole collection length, and electron collection length; $(\mu\tau)^*$, $(\mu\tau)_h$, and $(\mu\tau)_e$ is effective $\mu\tau$, hole $\mu\tau$, and electron $\mu\tau$ product; V_{bi} and V_a is the built-in potential of *pin* diode and applied voltage. Equation (3) presents that effective collection length increases as n_0 increases due to the increase of effective hole collection length l_p^*. This also leads to reduced recombination rate R in i layer.

$$R = \frac{pn}{\frac{pl_p^*}{v_p} + \frac{nl_n}{v_n}}. \tag{4}$$

Extracted parameters from curve fittings are summarized in Table II, where l_c^* increases with N-treatment as expected by Eq. (3). The ratio n_0/n_L are also obtained from the difference of l_c^*'s between untreated and N-treated. The thinner p layer shows a much larger enhancement in l_c^* than the

TABLE II. Extracted parameters from curve fitting of Fig. 7 using Eq. (3).

	V_{bi}(V)	$(\mu\tau)^*$(cm^2/V)	l_c^*(nm)	n_0/n_L
20 s untreated	0.71	8.61×10^{-9}	2436	0[a]
20 s N-treated	0.61	1.45×10^{-8}	3559	0.32
60 s untreated	0.80	7.51×10^{-9}	2404	0[a]
60 s N-treated	0.73	8.89×10^{-9}	2596	0.074

[a]These zeros are assumed values, that is, electron injection from p layer is not considered for untreated cases.

thicker one, which is due to the more injection of electrons from the p layer into the i layer. This is consistent with the larger QE enhancement for the thinner p layer. In addition, V_{bi} is reduced with nitrogen plasma treatment. However, the extracted values do not represent the real V_{bi} values of diodes because they are smaller than Voc. Extracted V_{bi}'s correspond to applied biases where QE values become zero, which means that the junction voltage drop at the onset of the disappearance of QE is larger than zero.

Our results revealed negligible efficiency improvement ($\sim$3.6%) with N-treated SnO_2:F; this is mainly due to reduced V_{bi} and increased R_s. Further optimization might not lead to drastic improvement in the efficiency of *pin* type a-Si solar cells because surface band bending of SnO_2:F results in trade-off between Jsc and Voc due to the change in V_{bi} as illustrated in Fig. 6. However, when we insert a buffer material with a band alignment causing hole accumulation at the buffer/p-a-SiC interface, carrier extraction from p-a-SiC and an increase of V_{bi} could be simultaneously obtained. As an example, one recent report on the efficiency improvement with WO_3 buffer between SnO_2:F and p-a-SiC, where simultaneous improvement of Jsc and Voc was observed,[7] supports this argument.

IV. CONCLUSION

Nitrogen treatment on SnO_2:F enhances carrier collection of a *pin* type a-Si solar cell in short wavelength regime, reduces V_{bi}, and increases R_s. These effects can be explained by the reversal of band bending at p-a-SiC caused by carrier depletion on the SnO_2:F surface. Optimization of the SnO_2:F surface treatment or insertion of high work function buffer material would lead to further efficiency improvement.

ACKNOWLEDGMENTS

This work was supported by a Korea Science and Engineering Foundation (KOSEF) grant funded by the Korea government (MEST) (2008-0062241), and the Brain Korea 21 Project, the School of Information Technology, KAIST in 2010.

[1]A. V. Shah, H. Schade, M. Vanecek, J. Meier, E. Vallat-Sauvain, N. Wyrsch, U. Kroll, C. Droz, and J. Bailat, Prog. Photovoltaics **12**, 113 (2004).
[2]K. Haga, K. Yamamoto, M. Kumano, and H. Watanabe, Jpn. J. Appl. Phys. **25**, L39 (1986).
[3]M. Kubon, E. Boehmer, F. Siebke, B. Rech, C. Beneking, H. Wagner, Sol. Energy Mater. Sol. Cells **41/42**, 485 (1996); H. Stiebig, F. Siebke, W. Beyer, C. Beneking, B. Rech, and H. Wagner, Sol. Energy Mater. Sol. Cells **48**, 351 (1997); J. Müller, O. Kluth, S. Wieder, H. Siekmann, G. Schöpe, W. Reetz, O. Vetterl, D. Lundszien, A. Lambertz, F. Finger, B. Rech, and H. Wagner, Sol. Energy Mater. Sol. Cells **66**, 275 (2001).
[4]J. C. Han, M. L. Tan, J. Q. Zhu, S. H. Meng, B. S. Wang, S. J. Mu, and D. W. Cao, Appl. Phys. Lett. **90**, 083508 (2007).
[5]Y. M. Li, F. Jackson, L. Yang, B. F. Fieselmann, and L. Russell, Mat. Res. Soc. Symp. Proc. **336**, 663 (1994).
[6]C. H. Lee and K. S. Lim, Appl. Phys. Lett. **72**, 106 (1998).
[7]L. Fang, S. J. Baik, K. S. Lim, S. H. Yoo, M. S. Seo, S. J. Kang, and J. W. Seo, Appl. Phys. Lett. **96**, 193501 (2010).
[8]S. J. Baik, S. J. Kang, and K. S. Lim, Appl. Phys. Lett. **97**, 122102 (2010).
[9]H. Schade, Z. E. Smith, J. H. Thomas III, and A. Catalano, Thin Solid Films **117**, 149 (1984); J.-M. Themlin, M. Chtaïb, L. Henrard, P. Lambin, J. Darville, and J.-M. Gilles, Phys Rev B **46**(4), 2460 (1992).
[10]M. Kunat, St. G. Girol, U. Burghaus, and Ch. Wöll, J. Phys. Chem. B **107**, 14350 (2003).
[11]C. L. Perkins, S.-H Lee, X. Li, S. E. Asher, and T. J. Coutts, J. Appl. Phys. **97**, 034907 (2005); H. Maki, I. Sakaguchi, N. Ohashi, S. Sekiguchi, H. Haneda, J. Tanaka, and N. Ichinose, Jpn. J. Appl. Phys., **42**(1), 75 (2003); S. Jiao, Y. Lu, Z. Zhang, B. Li, B. Yao, J. Zhang, D. Zhao, D. Shen, and X. Fan, J. Appl. Phys. **102**, 113509 (2007).
[12]S. S. Pan, C. Ye, X. M. Teng, H. T. Fan, and G. H. Li, Appl. Phys. A **85**, 21 (2006).
[13]R. S. Crandall, J. Appl, Phys. **53**(4), 3350 (1982); R. S. Crandall, J. Appl. Phys. **54**(12), 7176 (1983); B. W. Faughnan and R. S. Crandall, Appl. Phys. Lett. **44**(5), 537 (1984).
[14]S. S. Hegedus, Prog. Photovoltaics **5**, 151 (1997).
[15]S. Sriraman, S. Agarwal, E. S. Aydil, and D. Maroudas, Nature **418**, 62 (2002).
[16]J. H. Jang and K. S. Lim, Appl. Phys. Lett. **71**(13), 1846 (1997); S. Y. Myong and K. S. Lim, Appl. Phys. Lett. **86**, 033506 (2005).
[17]A. Nuruddin and J. R. Abelson, Thin Solid Films, **394**, 49 (2001).